Research Article | Vol. 28, No. 22 / 26 October 2020 / Optics Express 33673
Optics EXPRESS

Terahertz photoconductive waveguide emitter with excitation by a tilted optical pulse front

QAMAR-UL ISLAM,[1] FANQI MENG,[1,2] MARK D. THOMSON,[1] AND HARTMUT G. ROSKOS[1,3]

[1] *Physikalisches Institut, Johann Wolfgang Goethe-Universität, Frankfurt am Main, Germany*
[2] *fmeng@physik.uni-frankfurt.de*
[3] *roskos@physik.uni-frankfurt.de*

Abstract: We explore the tilted-pulse-front excitation technique to control the superradiant emission of terahertz (THz) pulses from large-area photonconductive semiconductor switches. Two cases are studied. First, a photoconductive antenna emitting into free space, where the propagation direction of the optically generated THz beam is controlled by the choice of the tilt angle of the pump pulse front. Second, a THz waveguide structure with an integrated photoconductive window for the generation of THz radiation, where the injection of the THz radiation into a waveguide mode is optimized by the pulse front tilt. By providing long interaction lengths, such a waveguide-based optical-pump/THz-probe set-up may provide a new platform for the study of diverse short-lived optically induced excitations.

1. Introduction

The application of tilted optical pulse fronts for the excitation of nonlinear phenomena has a long history. Initially introduced in 1981 for an improvement of the time resolution of optical pulse autocorrelation measurements [1], it was soon instrumental for the realization of traveling-wave lasing using molecular dye solutions as gain media [2,3]. Notably, it enabled efficient pump power conversion into amplified spontaneous emission from infrared-emitting dyes which suffer from a very short excited-state lifetime and hence a low fluorescence quantum yield [2]. Since, then, the technique has found abundant applications in such diverse fields of photonics as traveling-wave excitation of X-ray lasers, ultrafast electron diffraction, achromatic phase matching for sum and difference frequency generation, e.g. in noncollinear-optical parametric amplifiers (NOPA), and – probably the most famous of all – for the phase-matched generation of very intense single-cycle THz pulses by optical rectification in inorganic [4–9] and organic [10] crystalline solids. Such THz radiation sources are now a standard tool in nonlinear THz spectroscopy. For an overview of work on the application of tilted-pulse-front excitation published until 2010, see Ref. [11].

For the future, one can expect more applications of the technique for the investigation of short-lived excitations especially in the THz spectral regime. An example where tilted-pulse-front excitation appears promising, is the study of optically induced transient THz gain with experiments to be performed in a similar way as reported in Refs. [2,3]. For instance, THz gain has been predicted for graphene excited by intense laser pulses [12–14] and population inversion has been verified [15,16]. But direct measurements of the gain by amplification of THz pulses by conventional pump/probe spectroscopy has not been successful until now, since the maximum gain of graphene is only 2.3% per layer, which is easily lost beneath the noise level of amplifier-laser-based measurement systems. A second example is Bloch gain (dispersive gain), expected for superlattices (lateral and vertical) and other quantum well structures as a consequence of k-space bunching by scattering processes [17–21]. Weak gain in the infrared has been measured in the case of structures of quantum cascade lasers [22]. In vertical semiconductor superlattices, where the gain is predicted to be substantial in the THz frequency regime, the gain is rapidly lost by the ultrafast formation of bias field domains [23,24]. This has prevented the observation

#403161 https://doi.org/10.1364/OE.403161
Journal © 2020 Received 23 Jul 2020; revised 23 Sep 2020; accepted 23 Sep 2020; published 23 Oct 2020

Optics EXPRESS

of THz pulse amplification in transmission-type optical-pump/THz-probe experiments. The alternative of pumping by an optical pulse with tilted pulse front, procuring gain just-in-time to a THz pulse propagating along the superlattice planes, appears promising. A third example, where traveling-wave-type gain experiments may be used is the study of photoluminescence (PL) quenching mechanisms. A representative example is PL quenching of molecules which exhibit aggregation-induced emission (AIE) [25–27]. It has long been speculated that PL quenching is mediated by the rotational/vibrational motion of the individual molecules. It is tempting to investigate this hypothesis by the excitation of amplified spontaneous emission from the molecules and then to investigate whether the emission is disturbed by excitation of molecular motion with THz radiation. With such applications in mind, we explore in this report tilted-pulse-front excitation in a semiconductor model system, a distributed photoconductive emitter [28,29]. It consists of a gapped microstrip line on a GaAs substrate where the optical pulse excites electron-hole pairs in the slot-like gap region. The charge carriers are accelerated in an applied bias field emitting a burst of broadband THz radiation. If properly synchronized with the optical excitation, the emission occurs in a phase-matched superradiant way and leads to the formation of a THz pulse, which propagates along the optically pumped waveguide and is emitted into free space at its end facet.

2. THz beam steering

In a first test experiment without THz waveguiding, we explore superradiant emission from a large-area photoconductive antenna. The measurements are performed with a Ti:sapphire laser emitting 800-nm pulses with a duration of 100 fs at a repetition rate of 82 MHz. The experimental set-up is shown in Fig. 1. As per other pump-probe experiments, the laser beam is split into a pump beam to generate the THz pulses and a probe beam to detect them by balanced electro-optic sampling. Tilting of the pump pulse front, i.e. such that the wave-front (perpendicular to the diffracted rays) and the pulse-front across the beam no longer coincide [11], is achieved with

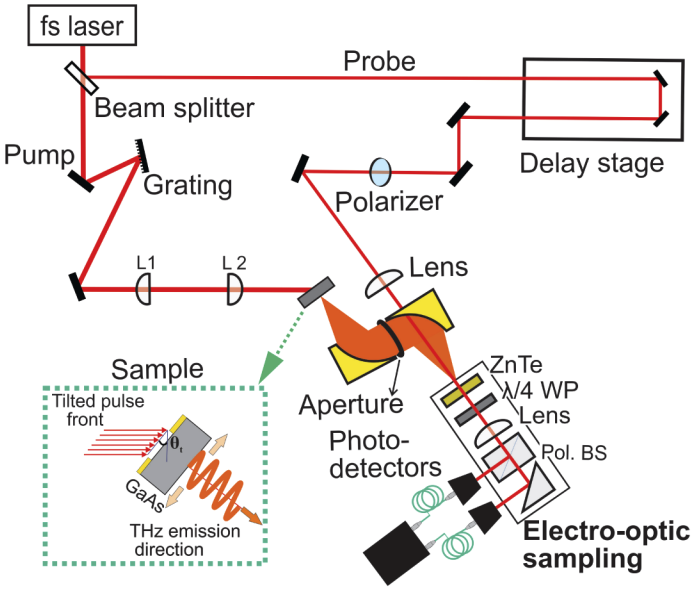

Fig. 1. Experimental set-up for the investigation of beam steering by tilted-pulse-front excitation. L1, L2 are two lenses in the telescope system, "$\lambda/4$ WP" stands for "quarter-wave plate", and "Pol. BS" for "polarization-selective beam splitter".

Optics EXPRESS

a reflective grating (1600 line/mm). A 4-f telescope consisting of two planoconvex lenses $L1$ and $L2$ with focal lengths $f_1 = 200$ mm and $f_2 = 250$ mm (magnification factor: 1.25 [6]) allows for more flexibility with the adjustment of the pulse-front tilt and helps to achieve both wave- and pulse-front flatness on the surface of the photoconductive antenna [30,31]. The collimated, p-polarized pump beam impinges onto the emitter with a power of 42 mW.

The photoconductive antenna consists of two Ti/Au patches (5/115-nm thick, each 3-mm wide, 4-mm long, unannealed) on top of a 380-μm-thick semi-insulating GaAs wafer, as shown in the inset of Fig. 1. The separation of the metal patches is 1 mm. Between them, a bias voltage of 300 V is applied. THz radiation polarized parallel to the GaAs surface is emitted. We collect and collimate the radiation propagating in a cone perpendicular to the sample with an off-axis gold-coated paraboloidal mirror (diameter: 50.8 mm, focal length from vertex: 76.2 mm) and focus the radiation with a second identical one onto the 500-μm-thick (110) ZnTe crystal for electro-optic detection. An iris (outer diameter: 57 mm; inner diameter: 24 mm) between the two paraboloidal mirrors serves to enhance the signal contrast upon changes of the tilt of the pump pulse front (for the optimal tilt angle, all THz radiation leaving the GaAs wafer transmits through the iris).

The pump beam (diffraction order $m = -1$) impinges onto the GaAs surface at an angle of 45°. The tilt angle of the pulse front is determined by the angle of incidence of the pump beam on the grating and by the magnification factor of the telescope [6,9]. With the angle of incidence changing from 14° to 33°, the tilt angle varies from 39° to 50°, which allows to control the emission direction of the THz pulses into the GaAs wafer. When the tilt angle (θ_t) is 45°, the pulse front of the pump beam is parallel with the semiconductor surface, and the THz beam is emitted perpendicular to the sample surface, as indicated in the inset of Fig. 1.

Figure 2 shows the measured time-domain traces (a) and their spectra (b) of the THz pulses for various tilt angles, and compares them with the reference pulse shape and spectrum measured for $\theta_t = 0°$ and THz pulse emission at 45° in reflection direction from the sample's front surface (pump power: 170 mW). Variation of θ_t gives the shortest THz pulses with the largest bandwidth and amplitude for $\theta_t = 45°$, as expected. Compared with the spectrum of the reference pulse, the

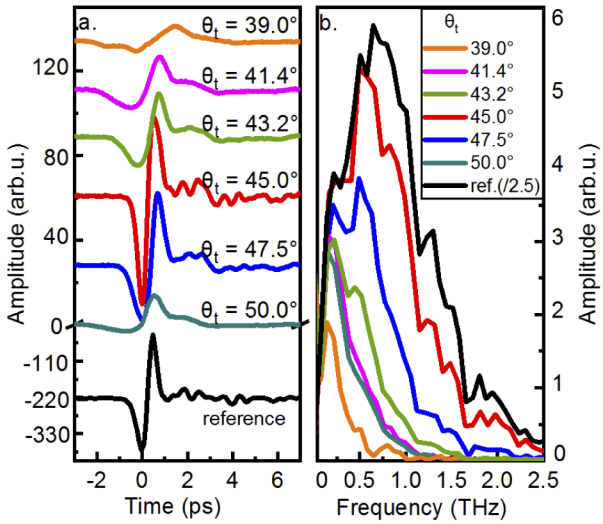

Fig. 2. Temporal waveforms (a) and spectra (b) of THz pulses collected from the optically excited GaAs photoconductive antenna at several values of the tilt angle θ_t of the pump pulse front. The temporal waveforms in (a) are shifted vertically for better visibility. Black solid lines are the temporal waveform and spectrum of a reference measurement.

Optics EXPRESS

bandwidth for this optimal case is reduced only moderately, the peak is shifted, however, to lower frequencies (from 0.65 THz to 0.5 THz).

3. Synchronized THz emission from a gapped microstrip line

We now come to the waveguide experiments. The measurement set-up is shown in Fig. 3. It is similar to that of the previous experiment, except that the pump beam now impinges onto the waveguide at normal incidence, and the THz radiation is collected at the end facet of the waveguide. The waveguide, schematically displayed in the inset of Fig. 3, consists of a Ti/Au metal layer (5/115-nm thick, 3.3-mm total width, 8-mm long, unannealed) with a slot window on top of a 380-μm-thick semi-insulating GaAs wafer and a 5-nm/115-nm-thick Ti/Au ground plane on its backside. The slot in the top metal has a width of 320 μm. It serves as a window for the optical excitation. It is covered with a semi-transparent Ni/Cr film (2-nm/2-nm thick) to allow optical beam penetration, while supporting the THz wave guiding of the neighboring thicker Ti/Au layer [32,33]. A voltage of 80 V is applied between the top and back metallic layers, such that the electric dipole moments of the photo-generated and field-accelerated charge carriers and the polarization of the emitted THz pulse are oriented perpendicular to the surface of the GaAs waveguide. One has to note that the semi-transparent layer is crucial for the experiment, as it ensures the presence of the bias field in the optically excited region of the GaAs; no THz emission was recorded from a sample without the semi-transparent layer.

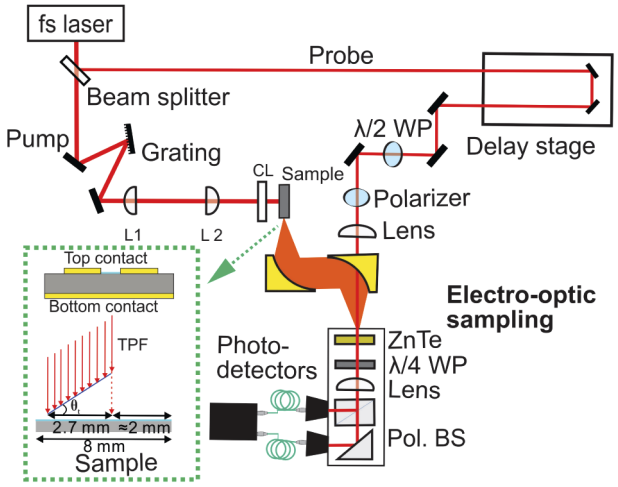

Fig. 3. Experimental set-up for the investigation of synchronization of the optical pump pulse and the THz pulse propagating in a gapped microstrip waveguide. "CL" stands for "cylindrical lens", "TPF" (in the inset) for "tilted pulse front".

For the phase-matched synchronization of the pump pulse and a given spectral component of the THz pulse, the group velocity of the optical pump pulse (here, the speed of light c_0 in air) and the phase velocity v_{THz} of the THz radiation in the waveguide have to fulfill the tilted-pulse-front condition [4,11]:

$$tan(\theta_t) = \frac{c_0}{v_{\mathrm{THz}}} \tag{1}$$

Under the synchronization condition, the pump pulse sweeps across the surface with the same velocity as that of the THz pulse propagating along the waveguide. If one assumes the THz pulse to be confined within the GaAs (no leakage through the slot window) and modal (plasmonic) modifications of the propagation speed to be negligible, then the effective refractive index of

Optics EXPRESS

the waveguide should be equal to the intrinsic refractive index of GaAs ($n_{\mathrm{THz}} \approx 3.6$; for the dispersion, see Ref. [34]), and the tilt angle is predicted to be about 74.5°. In order to reach such a large tilt angle, lens $L2$ in the telescope is replaced by a planoconvex lens with $f_2 = 70$ mm, which gives a magnification factor of 0.35. A cylindrical lens of 15-mm focal length is used to focus the pump beam into the slot of the waveguide. The length of the illuminated section of the slot is 2.7 mm, after which the THz pulse has to propagate another 2 mm to reach the end facet. Tuning of the tilt angle θ_t is achieved by changing the horizontal tilt of the grating and fine-tuning two subsequent mirrors to re-establish the beam axis approaching the sample (defined by two iris apertures in the beam path).

The THz transients measured at different tilt angles and the corresponding spectra are presented in Figs. 4(a) and (b), respectively. At a tilt angle of 74.5° (corresponding angle of incidence on the grating of 21°), one observes the strongest THz pulses with the largest bandwidth. Any small variation of θ_t leads to a loss of power and bandwidth. This indicates that the synchronization of the pulses is indeed achieved at this tilt angle, and confirms the assumptions made above with regard to the effective refractive index. The ringing in the trailing part of the best phase-matched pulse is consistent with the signature of THz absorption by water vapor in the air (the THz beam propagates in unpurged air). Similar ringing is observed in the corresponding transient in Fig. 2(a). In contrast to the spectra of Fig. 2(b), the peak frequency changes only weakly with θ_t, and it is located at lower frequency (at about 0.3 THz); however, in both case, frequencies above 1.5 THz are reached in the high-frequency tail of the spectrum for optimal phase-matching. The differences in the spectra may result from the influence of dispersion on the phase-matching, or from the modal properties of the THz beam, which may either propagate as a surface plasmon polariton along the top metal layer or as a double-sided plasmon polariton between the top and bottom metal, or as a mixture of both [35]. A precise angle-resolved analysis of the emission at the end facet of the waveguide might allow one to address the question of the modal character [35], but for such measurements, the THz signal turns out to be too weak. We also note that the THz pulse from the waveguide has about ten times less amplitude than the THz pulse from the photoconductive antenna. We attribute this difference mainly to the lateral divergence of the beam in the waveguide. The divergence is controlled by the constructive interference of the emission along the pumped segment of the slot and by the outer edges of the metal stripes. We have performed additional measurements with a second waveguide sample with wider waveguide stripes, but the same slot width (data not shown). There, the power is even lower, which we explain by a reduced lateral wave confinement. One should keep in mind that any radiation, which hits the end facet at an angle of more than 16°, experiences total internal reflection. Even for smaller angles, the out-coupled radiation may miss the collection cone of the first paraboloidal mirror. These effects are also likely to influence the spectral characteristics of the measured THz radiation. In order to improve the spectral fidelity, one could consider near-field detection [36,37] at the end facet of the waveguide.

In order to better understand our experimental results, we simulate the experiment with a simple 1D wave model for the total surface electric field emerging from the waveguide as a function of frequency and pulse-front tilt. This involves integrating the contribution from emission at each point $x \in [0, L]$ along the tilted-pulse-front beam profile, i.e.

$$\delta E(\omega, x) \propto P(\omega, x)\, d(L - x)\, e^{-i\, n_{\mathrm{THz}}(\omega/c_0)(L-x)}, \tag{2}$$

where

$$P(\omega, x) = p(\omega)\, e^{-i(\omega/c_0)x \tan\theta_t} \tag{3}$$

is the THz polarization (where $p(\omega)$ is determined from the phase-matched THz spectrum), and $d(L - x)$ represents the decay of the local emission with distance due to beam divergence. Here, we neglect waveguiding effects, due to the large width of the metal stripes and thick GaAs substrate. We note that in the THz frequency range, one does not expect any significant plasmonic

Optics EXPRESS

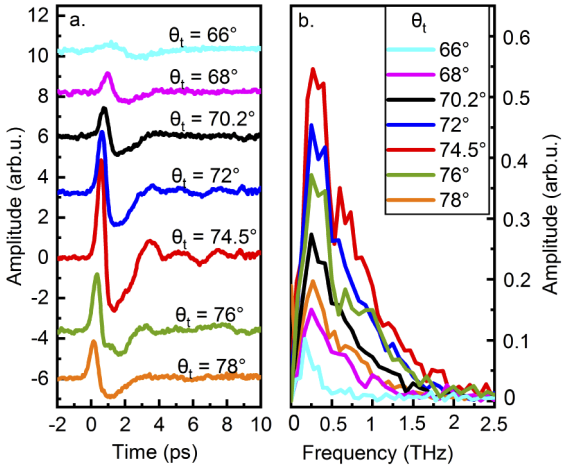

Fig. 4. Measured time-domain waveforms of the THz pulses (a) and corresponding spectra (b) extracted from a waveguide at different tilt angles of the pump pulse front. The temporal waveforms in (a) are vertically shifted for better visibility.

confinement of the field at the metal-dielectric interface. We then assume a decay factor factor $d(x) = \left(1 + (x/L_d)^2\right)^{-1}$, as per Gaussian beam divergence in two directions. The simulated decay curves are shown in Fig. 5(a), and show qualitative agreement with the experimental spectra, using values $L = 2.7$ mm, $L_d = 500$ μm and $n_{\mathrm{THz}} = 3.6$.

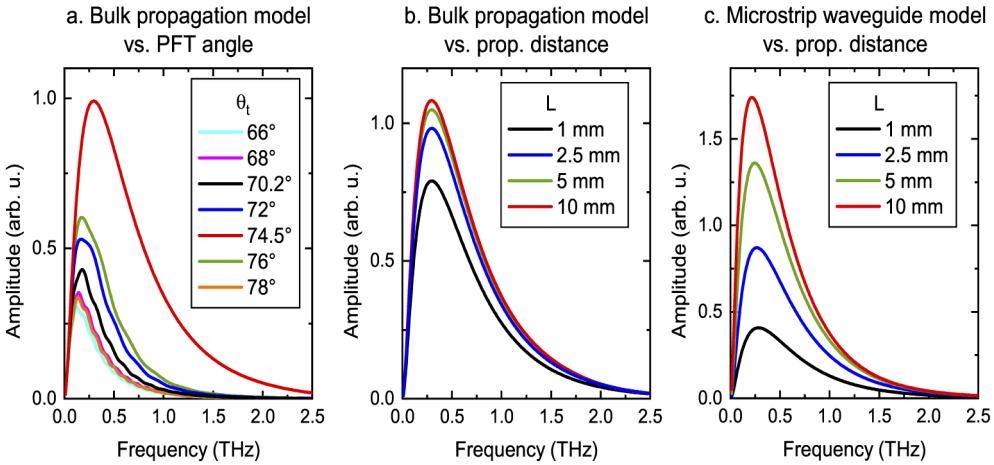

Fig. 5. Results of simulations with a 1D wave model: (a) Calculated THz spectra vs. pulse-front tilt angle assuming bulk wave divergence in the substrate. (b) Corresponding results for optimal pulse-front tilt angle vs. propagation distance L. (c) As per (b) for a proposed microstrip waveguide with sub-wavelength substrate thickness (see text for details).

It is interesting to consider how the performance could be enhanced by a more effective waveguiding of the emission, e.g. by using a microstrip waveguide with a strip width much smaller than that used here and a sub-wavelength substrate thickness. Such microstrip waveguides have demonstrated relatively low-loss, low-dispersion broadband guiding for their TEM mode in the THz region [38], although the dispersion can increase at lower frequencies as the mode

Optics EXPRESS

extends further into the surrounding air at the edges [39,40]. Here we consider a waveguide with strip width of w = 0.5 mm and GaAs substrate thickness of h = 10 μm, where h is chosen to provide a reasonable compromise between mode coupling from the emitting layer and the resultant mode attenuation coefficient. For such a sub-wavelength thickness, the TEM mode possesses a homogeneous mode distribution in the depth direction [38]. We perform a simulation of the surface field propagation similar to that above, only where the divergence term in Eq. (2) is replaced with the mode field attenuation factor for the TEM mode ($d(x) \rightarrow e^{-\frac{1}{2}\alpha x}$), where both the mode effective refractive index $n_{\mathrm{THz}}(\omega)$ and the absorption coefficient $\alpha(\omega)$ (due to metallic losses) can be calculated via the approximate analytic formulae in [41–43]. As we now consider a specific mode, we also apply a coupling factor from the emitting layer (thickness $h_p \sim 1$ μm) and the TEM mode, i.e. a power ratio of $\eta = h_p/h = 0.1$ and field ratio $\sqrt{\eta}$. For the microstrip waveguide considered, n_{THz} is within 0.01 of the bulk value of GaAs in the range 0.1-3 THz, while α varies from ~ 0.1-0.6 mm^{-1}. Here we concentrate on how the waveguiding can improve the total emission vs. the propagation distance L. In Fig. 5(b) we show the predicted spectra vs. L for our experimental structure based on the divergence properties used in Fig. 5(a). Here one sees that the coherent growth saturates already for L>2.5 mm due to the divergence. In comparison, in Fig. 5(c) we show the corresponding results for the microstrip waveguide. As can be seen, the coherent growth can be maintained for propagation distances of even up to L = 10 mm, before the mode attenuation saturates further growth. While the magnitude of surface field is still comparable between the two cases (due partly to the additional mode coupling factor $\sqrt{\eta}$ applied for the microstrip mode), we note that the output coupling of the homogeneous TEM mode should also be superior in practice. The performance of such a microstrip waveguide could be improved even further by introducing lateral confinement such as a ridge waveguide (where the waveguide dielectric also has a narrow width) as used in THz quantum cascade lasers [38].

Another interesting waveguide candidate for certain emission geometries would be a coplanar strip waveguide, e.g. with a lateral bias field between the two parallel strips on the substrate surface. This could allow a superior coupling to a more confined mode, and one can avoid the need for a semi-transparent metal strip for the optical excitation. However, in this case, the mode field has a substantial contribution parallel to the substrate surface, and hence is not well suited for coupling to the polarization (perpendicular to the substrate) of gain media such as graphene and quantum wells.

4. Conclusion

In this paper, we have demonstrated THz beam steering by phase-matched excitation of large-area photoconductive emitters with optical pump pulses exhibiting a tilted pulse front with adjustable tilt angle. The technique has been applied for free-space emission of THz pulses from a photoconductive antenna and for injection and guidance of THz pulses in a THz waveguide. The perspective of our work is that similar waveguide-based THz measurements can be used to probe short-lived optically induced excitations, such as THz gain in graphene, other van-der-Waals materials or superlattices, as well as relaxation mechanisms and dynamics in molecules.

Funding

Hessisches Ministerium für Wissenschaft und Kunst; Deutsche Forschungsgemeinschaft.

Acknowledgement

Q.-U.I. greatfully acknowledges funding by a scholarship of the HessenFonds of the Hessian Ministry for Science and Art. F.M. acknowledges funding by DFG (RO 770/40 and RO 770/41).

Optics EXPRESS

Disclosures

The authors declare that there are no conflicts of interest related to this article.

References

1. R. Wyatt and E. E. Marinero, "Versatile single-shot background-free pulse duration measurement technique, for pulses of subnanosecond to picosecond duration," Appl. Phys. **25**(3), 297–301 (1981).
2. H. Polland, T. Elsaesser, A. Seilmeier, W. Kaiser, M. Kussler, N. Marx, B. Sens, and K. Drexhage, "Picosecond dye laser emission in the infrared between 1.4 and 1.8 μm," Appl. Phys. B **32**(2), 53–57 (1983).
3. Z. Bor, S. Szatmári, and A. Müller, "Picosecond pulse shortening by travelling wave amplified spontaneous emission," Appl. Phys. B **32**(3), 101–104 (1983).
4. J. Hebling, G. Almási, I. Z. Kozma, and J. Kuhl, "Velocity matching by pulse front tilting for large-area THz-pulse generation," Opt. Express **10**(21), 1161 (2002).
5. A. G. Stepanov, J. Hebling, and J. Kuhl, "Efficient generation of subpicosecond terahertz radiation by phase-matched optical rectification using ultrashort laser pulses with tilted pulse fronts," Appl. Phys. Lett. **83**(15), 3000–3002 (2003).
6. H. Hirori, A. Doi, F. Blanchard, and K. Tanaka, "Single-cycle terahertz pulses with amplitudes exceeding 1 MV/cm generated by optical rectification in $LiNbO_3$," Appl. Phys. Lett. **98**(9), 091106 (2011).
7. L. Pálfalvi, J. Fülöp, G. Almási, and J. Hebling, "Novel setups for extremely high power single-cycle terahertz pulse generation by optical rectification," Appl. Phys. Lett. **92**(17), 171107 (2008).
8. J. A. Fülöp, L. Pálfalvi, S. Klingebiel, G. Almási, F. Krausz, S. Karsch, and J. Hebling, "Generation of sub-mJ terahertz pulses by optical rectification," Opt. Lett. **37**(4), 557 (2012).
9. F. Blanchard, B. E. Schmidt, X. Ropagnol, N. Thiré, T. Ozaki, R. Morandotti, D. G. Cooke, and F. Légaré, "Terahertz pulse generation from bulk GaAs by a tilted-pulse-front excitation at 1.8 μm," Appl. Phys. Lett. **105**(24), 241106 (2014).
10. M. Shalaby and C. P. Hauri, "Demonstration of a low-frequency three-dimensional terahertz bullet with extreme brightness," Nat. Commun. **6**(1), 5976 (2015).
11. J. A. Fülöp and J. Hebling, *Applications of Tilted-Pulse-Front Excitation* (Intech Europe, 2010), pp. 207–230, Recent Optical and Photonic Technologies.
12. V. Ryzhii, M. Ryzhii, and T. Otsuji, "Negative dynamic conductivity of graphene with optical pumping," J. Appl. Phys. **101**(8), 083114 (2007).
13. V. Ryzhii, M. Ryzhii, A. Satou, T. Otsuji, A. Dubinov, and V. Y. Aleshkin, "Feasibility of terahertz lasing in optically pumped epitaxial multiple graphene layer structures," J. Appl. Phys. **106**(8), 084507 (2009).
14. R. Jago, T. Winzer, A. Knorr, and E. Malic, "Graphene as gain medium for broadband lasers," Phys. Rev. B **92**(8), 085407 (2015).
15. T. Li, L. Luo, M. Hupalo, J. Zhang, M. C. Tringides, J. Schmalian, and J. Wang, "Femtosecond population inversion and stimulated emission of dense dirac fermions in graphene," Phys. Rev. Lett. **108**(16), 167401 (2012).
16. I. Gierz, J. C. Petersen, M. Mitrano, C. Cacho, I. E. Turcu, E. Springate, A. Stöhr, A. Köhler, U. Starke, and A. Cavalleri, "Snapshots of non-equilibrium dirac carrier distributions in graphene," Nat. Mater. **12**(12), 1119–1124 (2013).
17. A. A. Ignatov, K. F. Renk, and E. P. Dodin, "Esaki-Tsu superlattice oscillator: Josephson-like dynamics of carriers," Phys. Rev. Lett. **70**(13), 1996–1999 (1993).
18. E. Schomburg, N. Demarina, and K. F. Renk, "Amplification of a terahertz field in a semiconductor superlattice via phase-locked k-space bunches of Bloch oscillating electrons," Phys. Rev. B **67**(15), 155302 (2003).
19. H. Willenberg, G. H. Doehler, and J. Faist, "Intersubband gain in a bloch oscillator and quantum cascade laser," Phys. Rev. B **67**(8), 085315 (2003).
20. A. Lisauskas, E. Mohler, H. G. Roskos, and N. V. Demarina, "Towards superlattice terahertz amplifiers and lasers," in *Terahertz Frequency Detection of Materials and Objects*, R. E. Miles, X. C. Zhang, H. Eisele, and A. Krotkus, eds. (Springer, 2007), NATO Science for Peace and Security Series B – Physics and Biophysics, pp. 31–40.
21. T. Hyart, N. V. Alexeeva, J. Mattas, and K. N. Alekseev, "Terahertz Bloch oscillator with a modulated bias," Phys. Rev. Lett. **102**(14), 140405 (2009).
22. R. Terazzi, T. Gresch, M. Giovannini, N. Hoyler, N. Sekine, and J. Faist, "Bloch gain in quantum cascade lasers," Nat. Phys. **3**(5), 329–333 (2007).
23. P. G. Savvidis, B. Kolasa, G. Lee, and S. J. Allen, "Resonant crossover of terahertz loss to the gain of a Bloch oscillating InAs/AlSb superlattice," Phys. Rev. Lett. **92**(19), 196802 (2004).
24. A. Lisauskas, C. Blöser, R. Sachs, H. G. Roskos, A. Juozapavičius, G. Valušis, and K. Köhler, "Time-resolved photocurrent spectroscopy of the evolution of the electric field in optically excited superlattices and the prospects for Bloch gain," Appl. Phys. Lett. **86**(10), 102103 (2005).
25. J. Mei, N. L. Leung, R. T. Kwok, J. W. Lam, and B. Z. Tang, "Aggregation-induced emission: together we shine united we soar!" Chem. Rev. **115**(21), 11718–11940 (2015).
26. E. P. Parrott, N. Y. Tan, R. Hu, J. A. Zeitler, B. Z. Tang, and E. Pickwell-MacPherson, "Direct evidence to support the restriction of intramolecular rotation hypothesis for the mechanism of aggregation-induced emission: temperature resolved terahertz spectra of tetraphenylethene," Mater. Horiz. **1**(2), 251–258 (2014).

Optics EXPRESS

27. T. Zhang, Y. Jiang, Y. Niu, D. Wang, Q. Peng, and Z. Shuai, "Aggregation effects on the optical emission of 1,1,2,3,4,5-hexaphenylsilole (hps): a QM/MM study," J. Phys. Chem. A **118**(39), 9094–9104 (2014).
28. K. Victor, H. G. Roskos, and C. Waschke, "Efficiency of submillimeter-wave generation and amplification by coherent wave-packet oscillations in semiconductor structures," J. Opt. Soc. Am. B **11**(12), 2470–2479 (1994).
29. Q. Islam, F. Meng, H. Yuan, and H. G. Roskos, "THz emission from semiconductors using excitation by a tilted pulse front," Proc. SPIE **11279**, 1127910 (2020).
30. M. Kunitski, M. Richter, M. D. Thomson, A. Vredenborg, J. Wu, T. Jahnke, M. Schöffler, H. Schmidt-Böcking, H. G. Roskos, and R. Dörner, "Optimization of single-cycle terahertz generation in $LiNbO_3$ for sub-50 femtosecond pump pulses," Opt. Express **21**(6), 6826 (2013).
31. L. Tokodi, J. Hebling, and L. Pálfalvi, "Optimization of the tilted-pulse-front terahertz excitation setup containing telescope," J. Infrared, Millimeter, Terahertz Waves **38**(1), 22–32 (2017).
32. H. G. Roskos, M. C. Nuss, S. J. K. Leo, D. A. B. Miller, A. M. Fox, S. Schmitt-Rink, and K. Köhler, "Coherent submillimeter-wave emission from charge oscillations in a double-well potential," Phys. Rev. Lett. **68**(14), 2216–2219 (1992).
33. H. Kurz, H. G. Roskos, T. Dekorsy, and K. Köhler, "Bloch oscillations," Philos. Trans. R. Soc., A **354**(1717), 2295–2310 (1996).
34. D. Grischkowsky, S. Keiding, M. van Exter, and C. Fattinger, "Far-infrared time-domain spectroscopy with terahertz beams of dielectrics and semiconductors," J. Opt. Soc. Am. B **7**(10), 2006–2015 (1990).
35. S. Kohen, B. S. Williams, and Q. Hu, "Electromagnetic modeling of terahertz quantum cascade laser waveguides and resonators," J. Appl. Phys. **97**(5), 053106 (2005).
36. A. J. L. Adam, J. M. Brok, M. A. Seo, K. J. Ahn, D. S. Kim, J. H. Kang, Q. H. Park, M. Nagel, and P. C. M. Planken, "Advanced terahertz electric near-field measurements at sub-wavelength diameter metallic apertures," Opt. Express **16**(10), 7407 (2008).
37. R. Chakkittakandy, J. A. W. M. Corver, and P. C. M. Planken, "Quasi-near field terahertz generation and detection," Opt. Express **16**(17), 12794 (2008).
38. M. Martl, J. Darmo, D. Dietze, K. Unterrainer, and E. Gornik, "Terahertz waveguide emitter with subwavelength confinement," J. Appl. Phys. **107**(1), 013110 (2010).
39. K. W. Goossen and R. B. Hammond, "Modeling of picosecond pulse propagation in microstrip interconnections of integrated circuits," IEEE Trans. Microwave Theory Tech. **37**(3), 469–478 (1989).
40. H. G. Roskos, M. C. Nuss, K. W. Goossen, D. W. Kisker, A. E. White, K. T. Short, D. C. Jacobson, and J. M. Poate, "Propagation of picosecond electrical pulses on a silicon-based microstrip line with buried cobalt silicide ground plane," Appl. Phys. Lett. **58**(23), 2604–2606 (1991).
41. E. Hammerstad and O. Jensen, "Accurate models for microstrip computer-aided design," in *1980 IEEE MTT-S International Microwave Symposium Digest* (IEEE, 1980), pp. 407–409.
42. M. Kirschning and R. H. Jansen, "Accurate model for effective dielectric constant of microstrip with validity up to millimetre-wave frequencies," Electron. Lett. **18**(6), 272–273 (1982).
43. K. Gupta, R. Garg, and I. Bahl, *Microstrip Lines and Slotlines* (ARTECH HOUSE, INC, 1979).